On the cumulant analysis of EXAFS in crystalline solids

On the cumulant analysis of EXAFS in crystalline solids

Paolo Fornasini,[a]* Francesca Monti[b] and Andrea Sanson[a]

[a]Istituto Nazionale per la Fisica della Materia and Dipartimento di Fisica dell'Università di Trento, Via Sommarive 14, I-38050 Povo (Trento), Italy, and [b]Dipartimento Scientifico e Tecnologico, Università di Verona, Strada le Grazie, I-37134 Verona, Italy. E-mail: fornasin@science.unitn.it

The analysis of temperature-dependent EXAFS spectra based on the cumulant expansion is critically reviewed, seeking for accurate relations between EXAFS parameters and physical properties of crystals. The treatment is based on the distinction between the real and effective distribution of distances, and is divided into three logical steps. (*a*) The connection between lattice dynamics and cumulants C_n^* of the real distribution is studied and the extent of the usual approximations are numerically evaluated. Atomic vibrations perpendicular to the bond direction make the EXAFS thermal expansion larger than the crystallographic one; the difference is connected to a shift of the effective pair potential rather than to its asymmetry. Peculiar information on lattice dynamics of crystals can be obtained from accurate EXAFS measurements and their cumulant analysis. (*b*) The differences between cumulants of the real and effective distribution (C_n^* and C_n, respectively) are calculated for various physically realistic distributions. The largest discrepancy concerns the first cumulant: C_1^* measures the thermal expansion of the interatomic bond, while C_1 is a better estimate of the crystallographic thermal expansion. (*c*) The convergence properties of the cumulant series are discussed and some phenomenological procedures are suggested to monitor and possibly work out the connected failures of the cumulant method. Benefits and risks of the use of an effective pair potential are at last debated.

Keywords: EXAFS; cumulant analysis of EXAFS; anharmonicity; local thermal expansion.

1. Introduction

The standard treatment of thermal disorder in EXAFS through a harmonic Debye–Waller factor $\exp(-2k^2\sigma^2)$ (Lee *et al.*, 1981) has become inadequate with respect to the increasing accuracy of experimental data and analysis techniques. After the first pioneering studies of AgI (Boyce *et al.*, 1981) and CuBr (Tranquada & Ingalls, 1983), recent works have shown that anharmonic effects cannot be neglected even for systems like germanium (Dalba, Fornasini, Grazioli & Rocca, 1995) or GaAs (Dalba *et al.*, 1994).

The cumulant expansion approach to EXAFS (Bunker, 1983; Crozier *et al.*, 1988) facilitates both the theoretical interpretation (Frenkel & Rehr, 1993; Miyanaga & Fujikawa, 1994; Hung & Rehr, 1997; Yokoyama, 1998; Katsumata *et al.*, 2001) and the experimental analysis of anharmonic effects (Tranquada & Ingalls, 1983; Dalba *et al.*, 1993; Yokoyama *et al.*, 1997). The EXAFS cumulants C_n parametrize the distribution of interatomic distances and can be connected to the force constants of an effective pair potential (Stern *et al.*, 1991; Yokoyama *et al.*, 1996). Several review papers have been recently dedicated to the EXAFS Debye–Waller factor, including anharmonicity effects (Dalba & Fornasini, 1997; Fornasini, 2001).

The sensitivity of EXAFS to anharmonicity can be exploited to study the local thermal expansion (Tröger *et al.*, 1994). To this effect, both the first and third cumulant have often been considered equally sensitive to thermal expansion. This equivalence corresponds to considering the shift of the average value of the distance distribution as entirely due to the asymmetry of the effective potential. Accurate measurements on different crystals (Eisenberger & Brown, 1979; Dalba *et al.*, 1999) have, however, shown that the first cumulant is larger than the distance between the centres of thermal ellipsoids owing to the effect of atomic vibrations normal to the bond direction (Willis & Pryor, 1975; Ishii, 1992); as a consequence, EXAFS measures a thermal expansion larger that the crystallographic one. For germanium, the third cumulant reproduces the crystallographic thermal expansion through the ratio $C_3/2C_2$, suggesting that the thermal vibrations normal to the bond induce a positive shift of the effective pair potential, without affecting its asymmetry (Dalba *et al.*, 1999). For other crystals, however, the thermal expansion is not reproduced either by the first or by the third cumulant, and a negative shift of the effective potential is observed when the temperature increases (Dalba, Fornasini, Gotter & Rocca, 1995; Kamishima *et al.*, 1997; Dalba *et al.*, 1998).

These experimental results pose two questions, the first one concerning the actual accuracy of interatomic distances obtained from EXAFS, the second one concerning the possibility of obtaining peculiar information on local dynamics. The aim of this paper is to contribute to the advancement in these topics, seeking for a deeper understanding of the relations between the EXAFS parameters and the real structural and thermodynamical properties of crystals.

We will rely on the distinction between real and effective distributions (Bunker, 1983). Three logical steps will be singled out and separately considered. The first step is the reduction of two three-dimensional distributions of atomic positions into a one-dimensional real distribution of interatomic distances. This process is of geometrical nature, and depends on the vibrational properties of the crystal. The second step is the sampling of the real distribution by the photoelectron spherical wave, leading to an effective distribution of distances. This process depends on the EXAFS mechanism. The third step is the extraction of structural parameters from EXAFS spectra. This process depends on the analysis procedure. Following this schedule, we will distinguish three families of quantities: the cumulants of the real distribution, C_n^*, those of the effective distribution, C_n, and the polynomial coefficients obtainable from the analysis, $\tilde{C}_n$.

The cumulant method, as well as the distinction between real and effective distribution and the use of an effective pair potential, have been recently criticized (Filipponi, 2001). Actually, convergence problems can pose severe limitations to the cumulant method, in particular when dealing with structural disorder. Here we will only consider thermal disorder in the first coordination shell of crystals, and refer to temperature-dependent measurements analysed by the ratio method (Dalba *et al.*, 1993), taking the lowest-T spectrum (typically at liquid helium temperature) as reference for phase shifts, backscattering amplitudes and anelastic terms. The single scattering treatment in the plane-wave approximation is suitable for first-shell moderate thermal disorder. The soundness of this method has been checked on several systems, and has been recently confirmed by the accuracy of the results obtained on germanium (Dalba *et al.*, 1999) and their reproducibility by *ab initio* calculations (G. Birner, P. Pavone & D. Strauch, private communication). The distinction between real and effective distribution allows the separation of different effects depending on different causes and can facilitate the comparison of EXAFS results with the results from other techniques.

This paper is organized as follows. In §2 the connection between cumulants of the real distribution and the local vibrational properties is studied in the case of an ideally harmonic crystal. In §3, approximate relations between cumulants of the real and effective distributions are established. In §4 the connection between polynomial coefficients, $\tilde{C}_n$, and cumulants of the effective distribution, C_n, is explored. §5 contains some considerations about the effective potential, and §6 is dedicated to conclusions.

2. Real distribution of distances

Let us find the relations between the first cumulants C_n^* of the real distribution of distances $\rho(r, T)$ and the local thermal properties of the crystal. Here, $\rho(r, T)$ is the probability per unit radial length. We will restrict our treatment to an ideally harmonic crystal potential, so that the three-dimensional distributions of atomic positions are ellipsoids and there is no crystallographic thermal expansion.

The instantaneous distance r is connected to the equilibrium distance R by

$$r = R\left[1 + 2\Delta u_{\parallel}/R + \Delta u^2/R^2\right]^{1/2}, \tag{1}$$

where $\Delta\mathbf{u}$ is the instantaneous relative displacement and $\Delta u_{\parallel}$ is its projection parallel to the bond. Below we will consider also the projection $\Delta u_{\perp}$ perpendicular to the bond: $\Delta u^2 = \Delta u_{\parallel}^2 + \Delta u_{\perp}^2$. To simplify the notation, we will write Δu^2 instead of $(\Delta u)^2$.

The distribution $\rho(r, T)$ can be connected to a one-dimensional mean force pair potential, V_e (Cusack, 1987). In classical approximation,

$$\rho(r, T) = \exp\left[-\beta V_e(r)\right]\left\{\int \exp\left[-\beta V_e(r)\right] \mathrm{d}r\right\}^{-1}. \tag{2}$$

2.1. *Cumulants and lattice dynamics*

Following the procedure introduced by Beni & Platzman (1976) for the EXAFS Debye–Waller factor, we find approximate expressions of the first cumulants of $\rho(r, T)$ from canonical averages based on the power expansion of (1).

For the first cumulant $C_1^* = \langle r \rangle$, to first order and in harmonic approximation one has (Busing & Levy, 1964)

$$C_1^* \simeq R + \langle \Delta u_{\perp}^2 \rangle / 2R. \tag{3}$$

The thermal vibrations perpendicular to the bond cause a positive shift of C_1^* with respect to R and give rise to an apparent thermal expansion also for a harmonic crystal. By comparing the EXAFS C_1^* with R, the value $\langle \Delta u_{\perp}^2 \rangle$ for germanium has been recently obtained as a function of temperature (Dalba *et al.*, 1999), in good agreement with dynamical calculations based both on models (Nielsen & Weber, 1980) and *ab initio* (G. Birner, P. Pavone & D. Strauch, private communication).

The second cumulant $C_2^* = \langle (r - \langle r \rangle)^2 \rangle$ is the mean square relative displacement (MSRD). An approximate expression based on (1) is

$$C_2^* \simeq \langle \Delta u_{\parallel}^2 \rangle - \langle \Delta u_{\parallel}^2 \Delta u_{\perp}^2 \rangle / R^2 + \left[\langle \Delta u_{\perp}^4 \rangle - \langle \Delta u_{\perp}^2 \rangle^2\right]/4R^2, \tag{4}$$

where the first term on the right-hand side is the parallel MSRD, and the third term is the variance of the distribution of $\Delta u_{\perp}^2$. In the case of isotropy, $\langle \Delta u_{\perp}^2 \rangle = 2\langle \Delta u_{\parallel}^2 \rangle$ and (4) reduces to

$$C_2^* \simeq \langle \Delta u_{\parallel}^2 \rangle \left[1 - \langle \Delta u_{\parallel}^2 \rangle / R^2\right]. \tag{5}$$

It is customary to truncate (4) at the first term (Beni & Platzman, 1976),

$$C_2^* \simeq \langle \Delta u_{\parallel}^2 \rangle. \tag{6}$$

The relation between $\langle \Delta u_{\parallel}^2 \rangle$ and $\langle \Delta u_{\perp}^2 \rangle$ depends on the peculiar vibrational properties of the crystal. Only for an ideally isotropic crystal would the ratio $\gamma = \langle \Delta u_{\parallel}^2 \rangle / \langle \Delta u_{\perp}^2 \rangle$ be equal to 2 (Ishii, 1992); for the first shell of germanium the ratio increases with temperature to an asymptotic value of about 6 (Nielsen & Weber, 1980; Dalba *et al.*, 1999). While $\langle \Delta u_{\parallel}^2 \rangle$ can be directly obtained from EXAFS through (6), $\langle \Delta u_{\perp}^2 \rangle$ can only be calculated from (3), once R is known from other techniques.

The third cumulant, corresponding to the third central moment, $C_3^* = \langle (r - \langle r \rangle)^3 \rangle$, is the mean cubic relative displacement (MCRD). The lowest-order approximate expression based on (1) is

$$C_3^* \simeq (3/2R)\left[\langle \Delta u_{\parallel}^2 \, \Delta u_{\perp}^2 \rangle - \langle \Delta u_{\parallel}^2 \rangle \langle \Delta u_{\perp}^2 \rangle\right]. \tag{7}$$

The term within square brackets is the covariance between $\Delta u_{\parallel}^2$ and $\Delta u_{\perp}^2$, which is zero in harmonic approximation.

2.2. *Analytical form of the distribution*

Complementary information can be gained by studying the analytical expression of the distribution $\rho(r)$. We will follow the approach of Stern (1997), with the difference of a clear-cut distinction between real and effective distribution and the restriction to a harmonic crystal.

Let us first consider a Gaussian isotropic three-dimensional distribution $\rho(\mathbf{r})$, with $\sigma = \sigma_x = \sigma_y = \sigma_z$. For $\sigma \ll R$, the one-dimensional real distribution can be expressed as

$$\rho(r) \simeq \frac{1}{\sigma(2\pi)^{1/2}} \frac{r}{R} \exp\left[-\frac{(r-R)^2}{2\sigma^2}\right], \tag{8}$$

the first three cumulants are

$$C_1^* = R + \sigma^2/R, \tag{9}$$

$$C_2^* = \sigma^2 - \sigma^4/R^2, \tag{10}$$

$$C_3^* = 2\sigma^6/R^3, \tag{11}$$

and the position of the maximum is

$$r_{\max} = \left[R + (R^2 + 4\sigma^2)^{1/2}\right]/2 \simeq R + \sigma^2/R. \tag{12}$$

Equations (9) and (10) correspond to (3) and (5), respectively, since, in the case of isotropy, $\langle \Delta u_{\perp}^2 \rangle = 2\langle \Delta u_{\parallel}^2 \rangle = 2\sigma^2$. The right-hand sides of (9) and (12) are equal; the apparent thermal expansion induced by perpendicular atomic vibrations, (3), is to first order amenable to a shift of the maximum of the distribution, *e.g.* of the minimum of the effective pair potential V_e. The contribution of the asymmetry of V_e to the apparent thermal expansion, measured by the third cumulant, is negligible in comparison.

Let us now relax the condition of isotropy, and consider a Gaussian three-dimensional distribution $\rho(\mathbf{r})$, with variances $\sigma_z^2 = \sigma_{\parallel}^2$ along the bond direction and $\sigma_x^2 = \sigma_y^2 = \sigma_{\perp}^2$ in the normal plane. An approximate expression for the one-dimensional real distribution is (Stern, 1997)

$$\rho(r) \simeq \frac{1}{\sigma_{\parallel}(2\pi)^{1/2}} \exp\left[-\frac{(r-R)^2}{2\sigma_{\parallel}^2}\right]\left[1 + \frac{(r-R)}{R}\frac{\sigma_{\perp}^2}{\sigma_{\parallel}^2}\right]. \tag{13}$$

The first cumulant of this distribution,

$$C_1^* = R + \sigma_{\perp}^2/R, \tag{14}$$

is in agreement with (3), since $\langle \Delta u_{\perp}^2 \rangle = 2\sigma_{\perp}^2$. The second cumulant,

$$C_2^* = \sigma_{\parallel}^2 - \sigma_{\perp}^4/R^2, \tag{15}$$

is instead different from (4), suggesting that the approximations leading to (13) are too strong to allow a comparable accuracy.

2.3. *Numerical simulations*

The expressions for the cumulants and the maximum position of the real distribution given above are based on approximations. The errors introduced by these approximations depend on the overall degree of both thermal disorder and anisotropy. A quantitative evaluation has been attempted by a numerical simulation, consisting of the random sampling of a three-dimensional Gaussian distribution $\rho(\mathbf{r})$ to reconstruct the one-dimensional distribution $\rho(r)$ and calculate its parameters C_n^* and $r_{\max}$.

The width and anisotropy of the three-dimensional distribution were varied by imposing different values of $\sigma_z^2 = \langle \Delta u_\parallel^2 \rangle$ and of the ratio $\gamma = 2\sigma_x^2/\sigma_z^2 = 2\sigma_y^2/\sigma_z^2 = \langle \Delta u_\perp^2 \rangle / \langle \Delta u_\parallel^2 \rangle$. The results of the simulations are summarized in Figs. 1–4 as functions of the relative width C_2^*/R^2 and for different values of the ratio γ. Typical first-shell experimental values of C_2^*/R^2 at 400 K range from 0.0006 for germanium to 0.0025 for β-AgI. The ratio γ does not exceed 6 for the first shell of germanium and does not exceed 10 for the first shell of β-AgI.

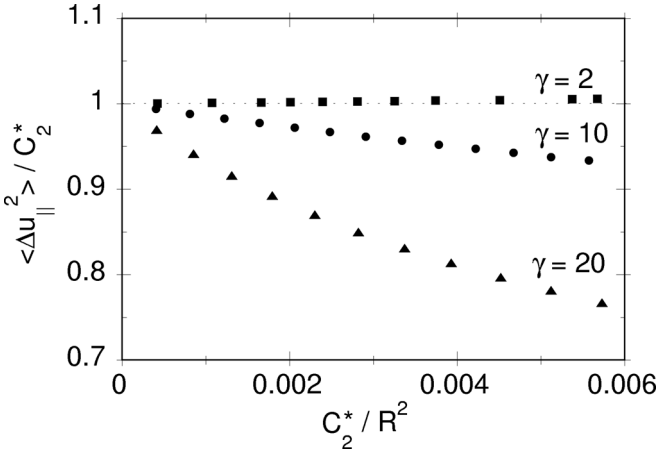

Figure 1
Ratio between parallel and total MSRD, $\langle \Delta u_\parallel^2 \rangle / C_2^*$, for different values of the ratio $\gamma = \langle \Delta u_\perp^2 \rangle / \langle \Delta u_\parallel^2 \rangle$.

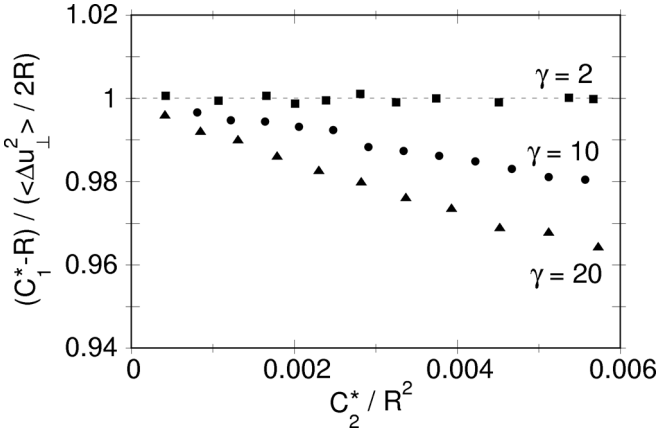

Figure 2
Ratio between the apparent thermal expansion $C_1^* - R$ and the first-order contribution $\langle \Delta u_\perp^2 \rangle / 2R$ [see equation (3)].

Fig. 1 refers to the MSRD, as expressed in (4), and shows the percentage error which is made by the usual approximation $C_2^* = \langle \Delta u_\parallel^2 \rangle$ in an ideal harmonic crystal. In the case of isotropy, $\gamma = 2$, the value $\langle \Delta u_\parallel^2 \rangle$ slightly exceeds C_2^*, as expected from (5). As soon as anisotropy is introduced, $\langle \Delta u_\parallel^2 \rangle$ becomes smaller than C_2^*, as an effect of the third term in (4). In any case, for first-shell realistic values of C_2^*/R^2 and γ, the difference does not exceed 0.5%. In real crystals, the discrepancy between C_2^* and $\langle \Delta u_\parallel^2 \rangle$ is augmented by anharmonicity effects (Dalba, Fornasini, Grazioli & Rocca, 1995; Strauch *et al.*, 1996).

Fig. 2 refers to the apparent thermal expansion $C_1^* - R$ induced by perpendicular vibrations, and shows the error caused by neglecting higher-order terms with respect to (3). The error increases with anisotropy γ, but is smaller than 1% for realistic first-shell cases.

Fig. 3 connects the apparent thermal expansion $C_1^* - R$ to the shift of the maximum position of the distribution, $r_{\max} - R$. In the case of anisotropy, the numerical simulations extend the results found analytically for isotropic distributions [equations (9) and (12)]. In the case of isotropy, the shift of the maximum position completely accounts for the apparent thermal expansion. The discrepancy

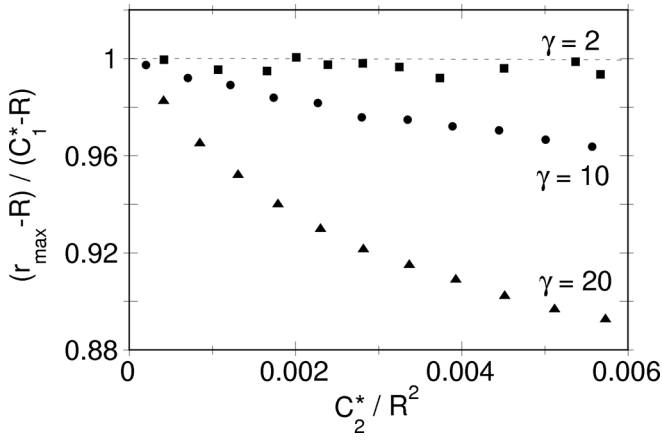

Figure 3
Ratio between the shift of the maximum of the distribution, $r_{\max} - R$, and the apparent thermal expansion $C_1^* - R$.

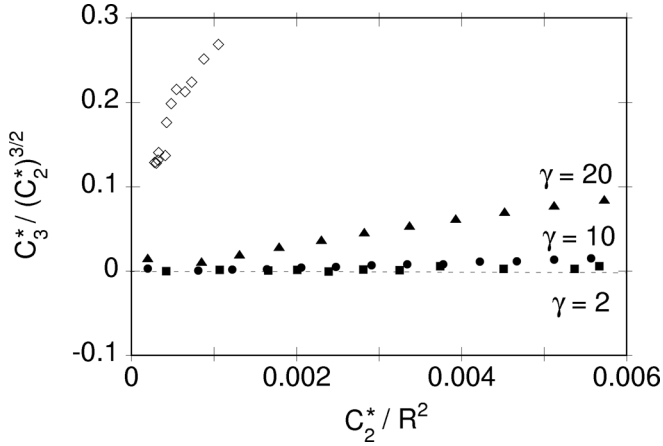

Figure 4
Numerical evaluation of the asymmetry parameter $C_3^*/(C_2^*)^{3/2}$ of the real distribution $\rho(r)$ for an ideally harmonic crystal (full symbols). The experimental values for the first shell of germanium are shown for comparison (open diamonds).

increases with anisotropy, but is always smaller than 4% for realistic first-shell cases.

The connection between cumulants of the real distribution and mean square relative displacements has been performed here for an ideal harmonic crystal. The results are nevertheless relevant also for real crystals. In a recent EXAFS work on germanium it was found that the ratio $C_3^*/2C_2^*$ very well reproduced the crystallographic thermal expansion, without being affected by atomic vibrations perpendicular to the bond (Dalba *et al.*, 1999). It was then argued that the apparent thermal expansion induced by perpendicular vibrations mainly corresponded to a positive shift of the minimum of the effective potential, and not to its asymmetry. The present numerical results confirm those assumptions. As further evidence, in Fig. 4 the asymmetry coefficients $C_3^*/(C_2^*)^{3/2}$ calculated for an ideally harmonic crystal (full symbols) are compared with the experimental values measured for germanium (open diamonds). The comparison confirms that the main contribution to the experimental third cumulant comes from the crystal anharmonicity, and the contribution of the vibrations perpendicular to the bond is negligible.

3. Effective distribution of distances

The effective distribution of distances measured by EXAFS,

$$P(r, k, T) = \rho(r, T)\exp[-2r/\lambda(k)]/r^2, \tag{16}$$

is generated by the weakening of the photoelectron wave with distance r, because of its spherical nature and finite mean free path $\lambda(k)$. The cumulants C_n are defined by the relation

$$\int_0^\infty P(r, k, T)\exp(2ikr)\,\mathrm{d}r = \exp\left[\sum_{n=0}^{\infty}(2ik)^n C_n(k, T)/n!\right]. \tag{17}$$

If the mean free path λ were a constant, then the phase and amplitude of EXAFS would depend only on odd and even k-independent cumulants, respectively. According to Bunker (1983), the weak k dependence of λ can be treated as a perturbation with respect to a central value λ_0, leading to the addition of even and odd cumulants into the expressions of EXAFS phase and amplitude, respectively. These additive terms, containing the k dependence of λ, can be non-negligible; however, they cancel when the analysis is performed by comparison with a suitable reference, as is the case of temperature-dependent measurements analysed by the ratio method. This analysis procedure justifies the usual assumption of a k-independent effective distribution,

$$P(r, \lambda_0, T) = \rho(r, T)\exp[-2r/\lambda_0]/r^2. \tag{18}$$

A rough quantitative estimate of the error induced by neglecting the k dependence of λ has been attempted utilizing the experimental values of C_2 for the first shell of germanium at 77 and 450 K. The results are shown in Fig. 5. Neglecting the k dependence of λ in the analysis causes an under-evaluation of the slope, *e.g.* of C_2 by about 40% at 77 K and 15% at 450 K. The error is, however, cancelled when the relative value $C_2(450\ \mathrm{K}) - C_2(77\ \mathrm{K})$ is considered.

3.1. *Analytical relations between cumulants*

We want now to investigate the connection between the cumulants of the real and effective distributions. To this effect, let us rewrite (18) as

$$\rho(r) = AP^*(r, \lambda)\,g(r, \lambda), \tag{19}$$

where $A = \int P(r, \lambda)\,\mathrm{d}r$, $P^*(r, \lambda) = P(r, \lambda)/A$ and $g(r, \lambda) = r^2\exp(2r/\lambda)$. The index 0 in λ_0 has been omitted for clarity. Let α_n and α_n^* be the moments of the effective and real distributions, respectively. By expanding $g(r, \lambda)$ as a Taylor series around $r = \alpha_1$, one finds the relations between the moments,

$$\begin{aligned}\alpha_n^* \simeq A\big[&g(\alpha_1, \lambda)\alpha_n + g(\alpha_1, \lambda)(\alpha_{n+1} - \alpha_1\alpha_n)\\ &+ g''(\alpha_1, \lambda)(\alpha_{n+2} - 2\alpha_1\alpha_{n+1} + \alpha_1^2\alpha_n)/2\\ &+ g'''(\alpha_1, \lambda)(\alpha_{n+3} - 3\alpha_1\alpha_{n+2} + 3\alpha_1^2\alpha_{n+1} - \alpha_1^3\alpha_n)/3!\\ &+ \ldots\big],\end{aligned} \tag{20}$$

where $g', g'', g''', \ldots$ indicate first, second, third, ... derivatives of $g(r, \lambda)$ with respect to r, and

$$\begin{aligned}A \simeq \big[&g(\alpha_1, \lambda) + g''(\alpha_1, \lambda)(\alpha_2 - \alpha_1^2)/2\\ &+ g'''(\alpha_1, \lambda)(\alpha_3 - 3\alpha_1\alpha_2 + 2\alpha_1^3) + \ldots\big]^{-1}.\end{aligned} \tag{21}$$

The cumulants are linear combinations of moments,

$$C_1 = \alpha_1, \tag{22}$$

$$C_2 = \alpha_2 - \alpha_1^2 \tag{23}$$

$$C_3 = \alpha_3 - 3\alpha_1\alpha_2 + 2\alpha_1^2, \tag{24}$$

$$C_4 = \alpha_4 - 3\alpha_2^2 - 4\alpha_1\alpha_3 + 12\alpha_2\alpha_1^2 - 6\alpha_1^4, \tag{25}$$

$$\ldots$$

From (20) one can obtain approximate relations connecting the cumulants. In particular, one recovers the expression for the first cumulants already derived by Freund *et al.* (1989) and currently utilized in EXAFS analyses,

$$C_1^* \simeq C_1 + (2C_2/C_1)(1 + C_1/\lambda). \tag{26}$$

3.2. *Numerical simulations*

A quantitative evaluation of the difference between the cumulants up to the third order has been attempted by direct calculations performed on a set of distributions with physically reasonable parameters: (*a*) Gaussian distributions with different values of position and width; (*b*) skewed distributions $\rho(r) = B\exp[-B(r - r_0)]$ with different values of position r_0 and skewness parameter B, convoluted with Gaussian distributions of different width; (*c*) two distributions derived from the excluded volume model for the I—Ag distance in

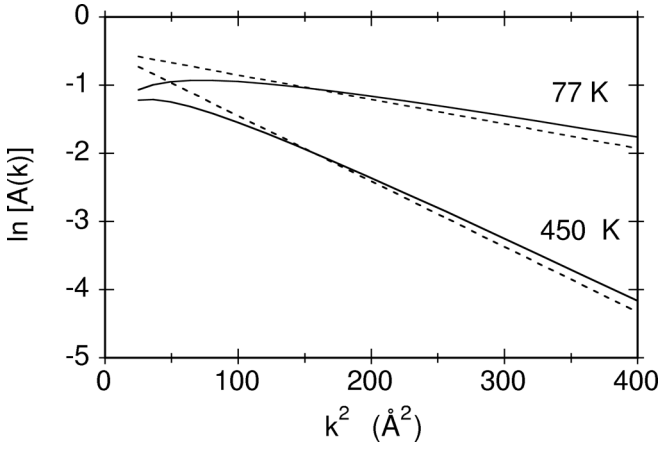

Figure 5
Logarithm of $A(k) = \exp(-2r/\lambda)\exp(-2k^2C_2)$ for the first shell of germanium. The experimental values of C_2 at 77 and 450 K have been utilized. Dashed lines refer to a constant λ value of 10 Å, continuous lines to a more realistic k-dependence, $\lambda = 2k/3 + 5/3$.

β-AgI at 300 and 370 K (Boyce *et al.*, 1981); (*d*) the distributions of the Cd—Se distance in CdSe obtained at various temperatures from 18 to 300 K from EXAFS measurements (Dalba *et al.*, 1998).

The results for the first cumulant are shown in Fig. 6. As expected, according to (26), C_1 is always smaller than C_1^*. The relative extent of the difference (open symbols, left-hand scale) increases with the relative width of the distribution. The difference, ranging from a few thousandths to more than one hundredth of an Ångström for realistic first-shell cases, can hardly be neglected. The upper part of the figure (full symbols, right-hand axis) shows that the difference is satisfactorily accounted for by the first-order term $(2C_2/C_1)(1 + C_1/\lambda)$ of (26).

The results for the second cumulant are shown in Fig. 7. The upper part of the figure (squares, upper axis) refers to real distributions $\rho(r)$ of Gaussian shape: C_2 is larger than C_2^*, the relative difference increasing with the width of the distribution. The lower part of the figure refers to asymmetric real distributions $\rho(r)$. A regular trend is evidenced if plotted against the adimensional variable $C_3^*/(C_2^*C_1^*)$, whose experimental first-shell values at 400 K range from 0.006 for germanium to 0.018 for β-AgI. C_2 is now smaller than C_2^*, the difference increasing with the asymmetry C_3^* and decreasing with the width C_2^*.

The results for the third cumulant are shown in Fig. 8. Here, only asymmetric real distributions have been considered. A regular trend is evidenced if the plot is performed against the adimensional variable $C_4^*/(C_3^*C_1^*)$, whose experimental value is about 0.1 for the first shell of β-AgI at 400 K. C_3 is smaller than C_3^*, the difference increasing with the flatness C_4^* and decreasing with the asymmetry C_3^*.

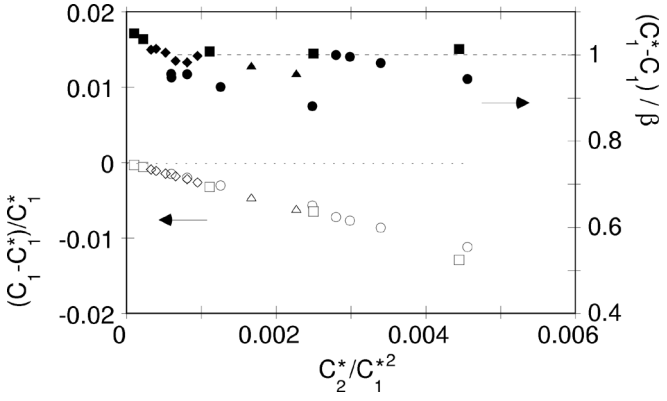

Figure 6
Relative difference between first cumulants of the effective and real distributions (open symbols, left-hand vertical axis), and ratio between the total difference $C_1^* - C_1$ and the first-order contribution $\beta = (2C_2/C_1)(1 + C_1/\lambda)$ (full symbols, right-hand vertical axis). Squares, circles, triangles and diamonds refer to Gaussian, skewed, excluded volume and CdSe distributions, respectively.

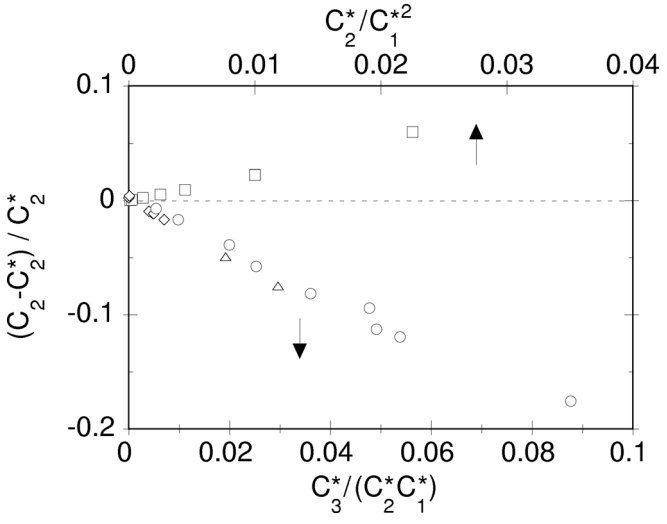

Figure 7
Relative difference between the second cumulant of the effective and real distributions. The upper horizontal axis refers to Gaussian distributions (squares). The lower axis refers to the other asymmetric distributions. Squares, circles, triangles and diamonds refer to Gaussian, skewed, excluded volume and CdSe distributions, respectively.

3.3. *EXAFS and local distance*

The interatomic distance is the basic physical quantity to which EXAFS is sensitive; its accurate determination is, however, far from trivial. According to (3), the first cumulant of the real distribution C_1^* is larger than the distance R between the centres of thermal ellipsoids owing to the effect of perpendicular vibrations. On the other hand, according to (26), the first cumulant of the effective distribution C_1 is smaller than C_1^*, owing to the weakening of the photoelectron wave with distance.

The two effects to a large extent compensate each other. To give an example, a comparison between R, C_1 and C_1^* for germanium is shown in Fig. 9 (Dalba *et al.*, 1999). C_1 is a better estimate of R than C_1^*. The temperature dependence of C_1^* measures the thermal expansion of the chemical bond between absorber and backscatterer atoms. According to (3), the difference between C_1^* and R contains peculiar information on $\langle \Delta u_\perp^2 \rangle$.

4. Experimental determination of cumulants

The number of independent parameters which can be obtained from an EXAFS spectrum is limited by the Δk and Δr windows (Stern, 1993). As a consequence, the cumulant expansion of (17) has to be truncated and only a finite number of polynomial coefficients $\tilde{C}_n$ can be derived from EXAFS analysis. For high-quality spectra, the cumulant order n can be as high as 6; usually $n \leq 4$.

The question arises of the accuracy by which the polynomial coefficients $\tilde{C}_n$ approximate the cumulants C_n. This problem was firstly addressed by Dalba *et al.* (1993) in a paper dedicated to

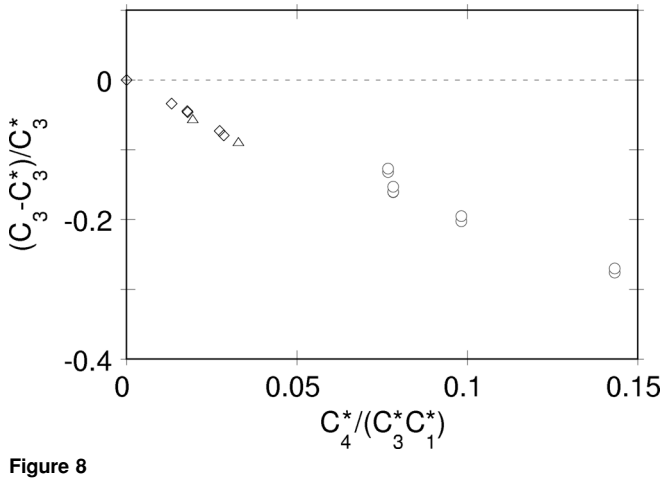

Figure 8
Relative differences between the third cumulant of the effective and real distributions. Circles, triangles and diamonds refer to skewed, excluded volume and CdSe distributions, respectively.

thermal disorder in β-AgI. There, a procedure was suggested, based on temperature-dependent measurements: the polynomial coefficients $\tilde{C}_n$ can be considered good estimates of the cumulants C_n if their temperature dependence is physically reasonable, *i.e.* Einstein-like for $\tilde{C}_2$, proportional to T^2 and T^3 for $\tilde{C}_3$ and $\tilde{C}_4$, respectively. Progressive deviations from expected behaviours when the temperature increases indicate the need for higher-order polynomial coefficients, if not the breaking off of the convergence properties. The soundness of this criterion was supported by tests on model distributions. In any case, only the first three cumulants are generally taken into account for their physical meaning, and for them the correspondence with the polynomial coefficients is important; higher-order polynomial coefficients are often introduced in the analysis only to guarantee the accuracy of the first three cumulants.

An EXAFS spectrum samples a portion of the characteristic function of $P(r, \lambda, T)$. The cumulant expansion is often utilized to extrapolate the characteristic function to $k = 0$ and to reconstruct, by Fourier transform, the distribution of distances (Stern *et al.*, 1992; Ono *et al.*, 1993). Tests on model distributions (Dalba *et al.*, 1993) have shown that, also when the polynomial coefficients are dramatically different from cumulants, as for skewed distributions with rather pathological convergence properties, they allow a reasonably accurate reconstruction of the starting distribution.

When the ratio method is utilized for the analysis of EXAFS spectra, only values $\Delta\tilde{C}_n$ relative to the reference spectrum can be obtained. If temperature-dependent measurements are available, absolute values of $\tilde{C}_n$ can be calculated by fitting the temperature dependence of $\Delta\tilde{C}_n$ with physical models. The use of the Einstein and Debye models for C_2 is well established (Dalba & Fornasini, 1997); classical T^2 and T^3 behaviours are used for third and fourth cumulants, respectively. Recently, low-temperature quantum deviations of the third cumulant from the classical behaviour have been experimentally observed (Dalba *et al.*, 1999), in agreement with theoretical calculations (Frenkel & Rehr, 1993; G. Birner, P. Pavone & D. Strauch, private communication).

The ratio method can be safely used when only one atomic species is present in the studied coordination shell and multiple scattering contributions are negligible. In spite of not giving absolute values of the cumulants, the ratio method has the advantage that backscattering amplitudes, phase shifts and anelastic terms cancel; also the spherical wave corrections and, as previously observed, the additive terms containing the k dependence of λ to a great extent cancel. Besides, the plots of phase differences and amplitude ratios at the basis of the ratio method are very sensitive to statistical noise and systematic errors, allowing a rather fast and easy assessment of the accuracy and reliability of experimental results.

The cumulant expansion and the ratio method have provided accurate and original results on thermodynamical properties of perfect crystals. The extension of these analysis techniques to systems affected by structural disorder is problematic, the main limitation being the poor convergence properties of the cumulant series. However, while the cumulant method is certainly useless for liquid systems (Filipponi, 2001), for amorphous solid systems the situation is not clear-cut. As a matter of fact, in an EXAFS study of amorphous germanium thin films (Dalba *et al.*, 1997) it was possible to separate the contributions of thermal and structural disorder, and the distribution reconstructed from cumulants was in good agreement with the distribution obtained by Filipponi & Di Cicco (1995) through a completely different approach. Recently, the cumulant method was again used to study the implantation-induced microstructural modifications in a-Ge (Ridgway *et al.*, 2000).

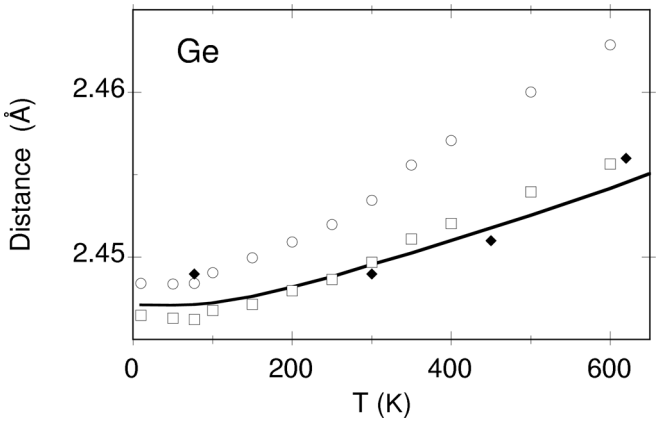

Figure 9
Temperature dependence of the EXAFS cumulants for the first shell of germanium (Dalba *et al.*, 1999): C_1 (squares) and C_1^* (circles). The continuous line is the crystallographic thermal expansion (Touloukian *et al.*, 1977). The diamonds are EXAFS distances quoted by Filipponi & Di Cicco (1995).

5. Effective pair potential

The basic result of the analysis of an EXAFS spectrum is the determination of a distribution of distances $\rho(r)$, or at least of its leading parameters. The further connection of the distributions $\rho(r, T)$ to an effective pair potential $V_e(r)$ through (2) requires some comments.

First of all, the effective potential $V_e(r)$ obtained by inversion of (2) should not be confused with the interaction potential between a pair of atoms. The effective potential $V_e(r)$ depends on the statistically averaged behaviour of all the atoms in the crystal, and can in principle depend on temperature (Mustre de Leon, 1992). The use of the effective potential, eliminating the trivial Maxwell Boltzmann temperature dependence of $\rho(r, T)$, allows the residual temperature dependence to be emphasized, which is connected to more subtle physical effects.

Secondly, (2) is based on the classical approximation; its use at low temperatures, where the classical approximation fails, leads to a meaningless potential $V_e(r)$, whose shape dramatically changes with temperature (Dalba *et al.*, 1998).

For the cases studied up to now, it seems reasonable to assume that, in the range of validity of the classical approximation, the temperature dependence of $V_e(r)$ is limited to its minimum position, the shape being unaffected. The temperature dependence of the first cumulants C_1^* is then a joint effect of the shift of the potential minimum and of the potential asymmetry. As it was previously demonstrated, the thermal vibrations perpendicular to the bond direction always produce a positive shift of the minimum position of $V_e(R)$.

In the case of germanium, it was possible to distinguish experimentally the two effects: the asymmetry of the potential $V_e(R)$, monitored by the ratio $C_3^*/2C_2^*$, fully accounts for the crystallographic thermal expansion of the crystal, while the positive shift of the potential minimum is due to the atomic perpendicular vibrations (Dalba *et al.*, 1999).

The situation is more complex in other systems. A negative shift of the minimum position of $V_e(r)$ has been experimentally observed in superionic conductors AgI (Dalba, Fornasini, Gotter & Rocca, 1995) and CuBr (Kamishima *et al.*, 1997). Correspondingly, the ratio $C_3^*/2C_2^*$ is unable to account for thermal expansion. The negative contribution to the potential shift is evidence of an anomalous local behaviour. The negative shift of CuBr and AgI has been recently

reproduced by theoretical investigations based on a cluster distortion coupling model (Ishii & Kamishima, 2001).

6. Conclusions

The cumulant analysis of EXAFS spectra can provide very accurate results on the local structure and dynamics of crystalline systems.

The highest accuracy, at least for relative values, is obtained when temperature-dependent measurements are performed down to liquid helium temperature and the data analysis is performed by the ratio method. In this way, the convergence properties of the cumulant series can be evaluated from the temperature dependence of the polynomial coefficients $\tilde{C}_n$ obtained from the analysis. Besides, the ratio method allows an efficient cancellation of unknown physical quantities, including the k dependence of the mean free path, and an easy evaluation of the quality of experimental data and of the reliability of final results.

Extracting the maximum of structural and dynamical information from EXAFS results requires a good knowledge of the relations connecting the cumulants C_n of the effective distribution to the cumulants C_n^* of the real distribution and to the physical properties of the crystal. These relations and their usual approximations have been quantitatively studied in this paper.

Particularly intriguing is the determination of the interatomic distance and its temperature dependence. The first cumulant of the real distribution, C_1^*, is larger than the crystallographic distance R; its temperature dependence measures the thermal expansion of the interatomic bond. The first cumulant of the effective distribution, C_1, has no direct physical meaning; in any case it can be considered a better estimate of the crystallographic distance R than C_1^*.

The understanding of the difference between EXAFS and crystallographic distances is necessary to assess the accuracy of structural parameters obtained from EXAFS. The study of crystalline model compounds is a sort of calibration for subsequent applications to more complex systems. Besides, a clear-cut definition of the EXAFS distance is important when accurate multiple-scattering calculations are attempted.

The different temperature dependence of C_1^* and R provides peculiar information on atomic vibrations perpendicular to the bond. This property, besides its fundamental interest for testing the phase relationships between eigenvectors of the dynamical matrix obtained from calculations, can be exploited to study phenomena in which perpendicular vibrations play a relevant role, like negative thermal expansion and order–disorder or displacive phase transitions.

Finally, the temperature dependence of the EXAFS effective pair potential can help in clarifying the relations existing between the local dynamical behaviour and the average thermodynamical properties of materials.

The authors are indebted to G. Dalba, R. Grisenti, F. Rocca and D. Diop for their long-term cooperation in experimental work, and to R. Gotter, D. Pasqualini, J. Purans, A. Kuzmin, S. a Beccara, D. Strauch and P. Pavone for helpful discussions.

References

Beni, G. & Platzman, P. M. (1976). *Phys. Rev. B*, **14**, 1514–1518.
Boyce, J. B., Hayes, T. M. & Mikkelsen, J. C. (1981). *Phys. Rev. B*, **23**, 2876–2896.
Bunker, G. (1983). *Nucl. Instrum. Methods*, **207**, 437–444.
Busing, W. R. & Levy, H. A. (1964). *Acta Cryst.*, **17**, 142–146.
Crozier, E. D., Rehr, J. J. & Ingalls, R. (1988). In *X-ray Absorption*, edited by D. C. Koningsberger & R. Prins. New York: Wiley.
Cusack, N. E. (1987). *The Physics of Structurally Disordered Matter.* Bristol: Adam Hilger.
Dalba, G., Diop, D., Fornasini, P. & Rocca, F. (1994). *J. Phys.Condens. Matter*, **6**, 3599–3608.
Dalba, G. & Fornasini, P. (1997). *J. Synchrotron Rad.* **4**, 243–255.
Dalba, G., Fornasini, P., Gotter, R. & Rocca, F. (1995*b*). *Phys. Rev. B*, **52**, 149–157.
Dalba, G., Fornasini, P., Grazioli, M. & Rocca, F. (1995*a*). *Phys. Rev. B*, **52**, 11034–11043.
Dalba, G., Fornasini, P., Grisenti, R., Pasqualini, D., Diop, D. & Monti, F. (1998). *Phys. Rev. B*, **58**, 4793–4802.
Dalba, G., Fornasini, P., Grisenti, R. & Purans, J. (1999). *Phys. Rev. Lett.* **82**, 4240–4243.
Dalba, G., Fornasini, P., Grisenti, R., Rocca, F., Chambouleyron, I. & Graeff, C. F. O. (1997). *J. Phys. Condens. Matter*, **9**, 5875–5888.
Dalba, G., Fornasini, P. & Rocca, F. (1993). *Phys. Rev. B*, **47**, 8502–8514.
Eisenberger, P. & Brown, G. S. (1979). *Solid State Commun.* **29**, 481–484.
Filipponi, A. (2001). *J. Phys. Condens. Matter*, **13**, R23–R60.
Filipponi, A. & Di Cicco, A. (1995). *Phys. Rev. B*, **51**,12322–12336.
Fornasini, P. (2001). *J. Phys. Condens. Matter*, **13**, 7859–7872.
Frenkel A. I. & Rehr, J. J. (1993). *Phys. Rev. B*, **48**, 585–588.
Freund, J., Ingalls, R. & Crozier, E. D. (1989). *Phys. Rev. B*, **39**, 12537–12547.
Hung, N. V. & Rehr, J. J. (1997). *Phys. Rev. B*, **56**, 43–46.
Ishii, T. (1992). *J. Phys. Condens. Matter*, **4**, 8029–8034.
Ishii, T. & Kamishima, O. (2001). *J. Phys. Soc. Jpn*, **70**, 159–166.
Kamishima, O., Ishii, T., Maeda, H. & Kashino, S. (1997). *Solid State Commun.* **103**, 141–144.
Katsumata, H., Miyanaga, T., Yokoyama, T., Fujikawa, T. & Ohta, T. (2001). *J. Synchrotron Rad.* **8**, 226–228.
Lee, P. A., Citrin, P. H., Eisenberger, P. & Kincaid, B. M. (1981). *Rev. Mod. Phys.* **53**, 769–806.
Miyanaga, T. & Fujikawa, T. (1994). *J. Phys. Soc. Jpn*, **63**, 1036–1052.
Mustre de Leon, J., Conradson, S. D., Batistić, I., Bishop, A. R., Raistrick, D., Aronson, M. C. & Garzon, F. H. (1992). *Phys. Rev. B*, **45**, 2447–2457.
Nielsen, O. H. & Weber, W. (1980). *J. Phys. C*, **13**, 2449–2460.
Ono, I., Yokoyama, T., Sato, H., Kaneyuki, K. & Ohta, T. (1993). *Jpn. J. Appl. Phys. Suppl.* **32**(2), 383–85.
Ridgway, M. C., Glover, C. J., Yu, K. M., Foran, G. J., Clerc, C., Hansen, J. L. & Nylandsted Larsen, A. (2000). *Phys. Rev. B*, **61**, 12586–12589.
Stern, E. A. (1993). *Phys. Rev. B*, **48**, 9825–9827.
Stern, E. A. (1997). *J. Phys. (Paris)*, C**2**, 137–140.
Stern, E. A., Livins, P. & Zhang, Z. (1991). *Phys. Rev. B*, **43**, 8850–8860.
Stern, E. A., Ma, Y., Hanske-Petitpierre, O. & Bouldin, C. E. (1992). *Phys. Rev. B*, **46**, 687–694.
Strauch, D., Pavone, P., Nerb, N., Karch, K., Windl, W., Dalba, G. & Fornasini, P. (1996). *Physica B*, **219/220**, 436–438.
Tranquada, J. M. & Ingalls, R. (1983). *Phys. Rev. B*, **28**, 3520–3528.
Touloukian, Y. S., Kirby, R. K., Taylor, R. E. & Desay, P. D. (1977). *Thermophysical Properties of Matter*, Vol. 13. New York: Plenum.
Tröger, L., Yokoyama, T., Arvanitis, D., Lederer, T., Tischer, M. & Baberschke, K. (1994). *Phys. Rev. B*, **49**, 888–903.
Willis, B. T. M. & Pryor, A. W. (1975). *Thermal Vibrations in Crystallography.* Cambridge University Press.
Yokoyama, T. (1998). *Phys. Rev. B*, **57**, 3423–3432.
Yokoyama, T., Ohta, T, & Sato, H. (1997). *Phys. Rev. B*, **55**, 11320–11329.
Yokoyama, T., Yonamoto, Y., Ohta, T. & Ugawa, A. (1996). *Phys. Rev. B*, **53**, 6111–6122.